Colloids and Surfaces B: Biointerfaces 114 (2014) 363–371

Contents lists available at ScienceDirect

Colloids and Surfaces B: Biointerfaces

journal homepage: www.elsevier.com/locate/colsurfb

Biological activity of antibacterial peptides matches synergism between electrostatic and non electrostatic forces

Ana M. Bouchet[a], Nancy B. Iannucci[b,c], María B. Pastrian[b], Osvaldo Cascone[b], Nuno C. Santos[d], Edgardo A. Disalvo[a], Axel Hollmann[a,d,e,*]

[a] Laboratory of Biointerfaces and Biomimetic Systems, CITSE—University of Santiago del Estero, 4200 Santiago del Estero and CONICET, Argentina
[b] School of Pharmacy and Biochemistry, University of Buenos Aires, Buenos Aires 1113, Argentina
[c] Therapeutic Peptides Research and Development Laboratory, Chemo-Romikin, 1605 Buenos Aires, Argentina
[d] Instituto de Medicina Molecular, Faculdade de Medicina, Universidade de Lisboa, Av. Prof. Egas Moniz, 1649-028 Lisbon, Portugal
[e] Laboratory of Molecular Microbiology, Institute of Basic and Applied Microbiology, University of Quilmes, B1876BXD Bernal, Argentina

ARTICLE INFO

Article history:
Received 14 August 2013
Received in revised form 7 October 2013
Accepted 16 October 2013
Available online 30 October 2013

Keywords:
Antimicrobial peptide
Lysozyme
Peptide–membrane interactions,
Hydrophilic–hydrophobic synergism

ABSTRACT

Substitution of Ala 108 and Ala 111 in the 107–115 human lysozyme (hLz) fragment results in a 20-fold increased anti-staphylococcal activity while its hemolytic activity becomes significant (30%) at very high concentrations. This analog displays an additional positive charge near the N-terminus (108) and an extra Trp residue at the center of the molecule (111), indicating that this particular amino acid sequence improves its interaction with the bacterial plasma membrane. In order to understand the role of this arrangement in the membrane interaction, studies with model lipid membranes were carried out.

The interactions of peptides, 107–115 hLz and the novel analog ([$K^{108}W^{111}$]107–115 hLz) with liposomes and lipid monolayers were evaluated by monitoring the changes in the fluorescence of the Trp residues and the variation of the monolayers surface pressure, respectively. Results obtained with both techniques revealed a significant affinity increase of [$K^{108}W^{111}$]107–115 hLz for lipids, especially when the membranes containing negatively charged lipids, such as phosphatidylglycerol. However, there is also a significant interaction with zwitterionic lipids, suggesting that other forces in addition to electrostatic interactions are involved in the binding. The analysis of adsorption isotherms and the insertion kinetics suggest that relaxation processes of the membrane structure are involved in the insertion process of novel peptide [$K^{108}W^{111}$]107–115 hLz but not in 107–115 hLz, probably by imposing a reorganization of water at the interphases.

In this regard, the enhanced activity of peptide [$K^{108}W^{111}$]107–115 hLz may be explained by a synergistic effect between the increased electrostatic forces as well as the increased hydrophobic interactions.

1. Introduction

Antimicrobial peptides (AMPs) are produced by almost all species of living beings as a component of their innate non-specific defense against infections [1–4]. AMPs are typically short peptides with consensus amphiphilic attributes represented by positively charged and hydrophobic amino acids. The mixed cationic and hydrophobic composition of AMPs makes them well suited for interacting with, and perturbing microbial plasmatic membranes, which typically present anionic surfaces, rich in lipids such as phosphatidylglycerol or cardiolipin oriented towards the outer environment of the bacteria [5]. The lethal step in most cationic AMPs (CAMPs) is the disruption of the microbial plasma membrane. This process is accomplished in two steps: membrane binding, predominantly governed by electrostatic interactions, and membrane insertion/permeation, related to the hydrophobicity of the peptide, which gives the capacity of partitioning into the microbial plasma membrane [5]. CAMPs are very important resources for human therapeutics as lead compounds to counteract the current drug resistance development [6–9].

The target of most CAMPs is the microbial plasma membrane, causing its perturbation and/or permeabilization. This target makes difficult the microbial-resistance development, becoming CAMPs excellent candidates to counteract the resistance spread. For this reason, model membrane systems, such as lipid vesicles, have been used for three decades to explore the structure, function and mechanism of AMPs [10,11]. Yet, despite a huge amount of work a consensus in the understanding of AMPs action in synthetic bilayers

* Corresponding author. Tel.: +351 217999480; fax: +351 217999477.
E-mail address: ahollmann@fm.ul.pt (A. Hollmann).

0927-7765/$ – see front matter © 2013 Elsevier B.V. All rights reserved.
http://dx.doi.org/10.1016/j.colsurfb.2013.10.025

Fig. 1. Sequence alignment of 107–115 hLz and [$K^{108}W^{111}$]107–115 hLz, and the well know AMP indolicidin [64]. Color code: blue, aliphathic residues and proline; red, aromatic residues; and green, polar and charged residues. (For interpretation of the references to color in this figure legend, the reader is referred to the web version of this article).

is still lacking. A way to get an insight on the antimicrobial activity of peptides is to elucidate the mechanism of the AMP-induced bilayer destabilization. In this regard, it is important to identify the AMPs features necessary for the display activity, enabling the design of more potent and simpler, i.e., less expensive, AMPs [12].

Recently, an improved analog derived from the 107–115 human lysozyme fragment (107–115 hLz), an AMP with well known antibacterial activity against both Gram-positive and Gram-negative microorganisms [13], was developed by a straightforward strategy, involving the sequential substitutions of both alanine residues (108 and 111) [14] (Fig. 1A). This simple strategy involved the screening of 16, 107–115 hLz analogs. Since small pharma and biotech firms took the challenge of antimicrobial development [15], low investment-venture procedures are welcome.

The novel peptide [$K^{108}W^{111}$]107–115 hLz resulted in a 20-fold increase in the anti-staphylococcal activity while its hemolytic activity resulted significant at 10-fold its MIC [14]. Furthermore, the conformational insight assessed by far-UV circular dichroism in the presence of structure-inducing agents, highlights the role of the peptide secondary structure and the distribution of polar/non-polar residues for its effective interaction with the bacterial plasma membrane (data not shown). This peptide might adopt an extended amphipatic conformation; with segregation of the charged-polar residues form the non-polar residues in order to improve its interaction with lipidic micelles which mimic the bacterial plasma membranes.

In this article, we aim to characterize comparatively the interaction of the lead peptide, 107–115 hLz, and its improved analog, [$K^{108}W^{111}$]107–115 hLz, with biomembranes composed by charged and non-charged lipids. These assays might help to further understand the structure–activity relationship (SAR) of this novel peptide and the role of each substitution.

Our approach involves a series of studies to determine the partition and the location of both peptides, the influence of electrostatic charges at the membrane surface on the partition and the membrane-structure changes induced by the peptides.

2. Material and methods

2.1. Lipids

The zwitterionc lipids POPC (1-palmitoyl-2-oleyl-*sn*-glycero-3-phosphocholine), DMPC (1,2-dimyristoyl-*sn*-glycero-3-phosphocholine) DOPC (1,2-dioleoyl-*sn*-glycero-3-phosphocholine) and positively charged lipids POPG (1-palmitoyl-2-oleoyl-*sn*-glycero-3-phospho-1′-rac-glycerol), and DMPG (1,2-dimyristoyl-*sn*-glycero-3-phospho-1′-rac-glycerol) were purchased from Avanti Polar Lipids (Alabaster, AL, USA). 5NS (5-DOXYL-stearic acid) and 16NS (16-DOXIL-stearic acid) were purchased from Sigma.

2.2. Peptide synthesis, purification and identification

Peptides were obtained by solid phase synthesis using the Fmoc *N*α-protection strategy, according to Kates and Albericio [16]. Amide resin was the solid support to provide amide peptides. Tetrafluoroborato de *N*-[(1*H*-benzotriazol-1-yl)(dimetilamino)metilen]-*N*-metilmetanamonio (TBTU) and *N*,*N*-diisopropiletilamina (DIEA) were the coupling reagents. MBHA (4-Methylbenzhydrylamine) rink amide resin, Fmoc amino acids, and coupling reagents were purchased form Peptides International (Louisville, KY, USA). Peptides were deprotected and cleaved from the resin using trifluoroacetic acid (TFA):H_2O:triisopropylsilane (TIS) (95:2.5:2.5) mixture for 3 h at room temperature. Peptides were purified by RP-HPLC on a Bio Basic-18 column (Thermo Scientific, USA). Peptide elution was performed using a linear gradient of 10–55% acetonitrile in water containing 0.05% of TFA, during 45 min, at 1 ml/min flow rate. Peptides were identified by MALDI-MS in a 4800 MALDI TOF/TOF plus equipment (Applied Biosystems MDS SCIEX, USA).

2.3. Surface pressure

Changes on the surface pressure of lipid monolayers induced by 107–115 hLz and [$K^{108}W^{111}$]107–115 hLz were measured in a Kibron Langmuir–Blodgett trough, at constant temperature ($25 \pm 0.5\,^{\circ}C$). The surface of the buffer solution contained in a Teflon trough of fixed area was exhaustively cleaned by surface aspiration. Then, a chloroform solution of lipids was spread on this surface to reach surface pressures of 20.5 ± 1 mN/m. Peptide solutions were injected in the subphase and the changes of surface pressure were recorded until a constant value was reached. The surface pressure of the air–water interface upon injecting the highest concentration of each peptide was below 14 mN/m. For this reason, the lowest initial surface pressure of the lipid monolayers before the addition of the peptides to the subphase was above that value. In this condition, the changes in the surface pressure observed upon the injection of the peptide solutions could can be ascribed to an effect of the peptide on the monolayer, altering its interfacial tension.

Pressure data obtained were fitted with follow equation:

$$\theta = \frac{\Delta\Pi}{\Delta\Pi_{\max}} = \frac{[\text{peptide}]^n}{k_d + [\text{peptide}]^n} \quad (1)$$

where θ corresponds to the degree of coverage, $\Delta\Pi$ is the surface pressure shift, [peptide] is the peptide concentration, n is the heterogeneity parameter describing the width of energy distribution and k_d is the dissociation constant.

2.4 Relaxation coefficient (r) in diffusional process

The kinetics of peptides penetration was followed using:

$$\Delta\Pi = k^r \quad (2)$$

from where the constants k and r [17] were determined.

Regression analyses of the $\Delta\Pi$ vs. $\sqrt{}$time curves were performed to determine the values of r, with Graphpad Prism, by minimizing the root mean square error between the experimental data rate and the model equation.

2.5. Fluorescence spectroscopy measurements

Since peptides 107–115 hLz and [$K^{108}W^{111}$]107–115 hLz contain 2 and 3 tryptophan residues, respectively, fluorescence techniques results suitable tools for the analyses of these molecules. The working buffer was HEPES 10 mM pH 7.4 in NaCl 150 mM. Peptides 107–115 hLz and [$K^{108}W^{111}$]107–115 hLz (250 μM) and Trp (500 μM) stock solutions were prepared in buffer. Membrane partition and fluorescence quenching studies were carried out in a Varian Cary Eclipse fluorescence spectrophotometer (Mulgrave, Australia). The fluorescence spectral characterization of peptides

and Trp was performed at 280 nm excitation wavelength, except for the quenching experiments that was performed at 290 nm to minimize the relative quencher/fluorophore light-absorption ratios. For the quenching experiments, fluorescence emission was collected at 350 nm (fixed wavelength). For the partition studies integrated spectra from 310 to 450 nm were used. Typical spectral bandwidths were 5 nm for excitation and 10 nm for emission. Excitation and emission spectra were corrected for wavelength-dependent instrumental factors [18,19]. During the quenching and partition experiments, emission was also corrected for successive dilutions, scatter [19] and simultaneous light absorptions of quencher and fluorophore.

2.6. Partition coefficient determination

Large unilamellar vesicles (LUV) were prepared by extrusion methods, as described elsewhere [20,21].

Membrane partition studies were performed by successive additions of small amounts of different lipid systems to a 5 μM peptide solution, with 10 min incubation at 25 °C. Lipid systems included: DMPC, DMPC:POPG (5:1), DMPC:POPG (2.5:1) and POPC:POPG (2.5:1). The partition coefficients (K_p) were calculated fitting the experimental data into equation 3 [22]:

$$\frac{I}{I_W} = \frac{1 + K_p \gamma_L \frac{I_L}{I_W} [L]}{1 + K_p \gamma_L [L]} \quad (3)$$

where I_W and I_L are the fluorescence intensities in aqueous solution and in lipid, respectively, γ_L is the molar volume of the lipid [23] and [L] its concentration.

2.7. Acrylamide quenching

The fluorescence quenching of peptides 107–115 hLz and [$K^{108}W^{111}$]107–115 hLz (5 μM) by acrylamide was measured in buffer and in the presence of POPC:POPG (2.5:1) LUV (3 mM), by successive additions of small volumes of the quencher stock solution, ranging from 0 to 60 mM [24]. Each spectrum was recorded after 10 min incubation. Quenching data were analyzed using the Stern–Volmer equation [25]:

$$\frac{I_0}{I} = 1 + K_{SV} \times [Q] \quad (4)$$

where I and I_0 are the fluorescence intensities of the sample in the presence and absence of quencher, respectively, K_{SV} is the Stern–Volmer constant and [Q] is the quencher concentration.

2.8 5NS and 16NS quenching

Fluorescence quenching assays with the lipophilic probes 5NS and 16NS were carried out at the same peptide and lipid concentrations used for the acrylamide quenching study. Briefly, by successive additions of small amounts of these quenchers in ethanol solution to the peptide samples in POPC:POPG (2.5:1), keeping the ethanol concentration below 2% (v/v) [26]. The effective lipophilic quencher concentration in the membrane was calculated from the partition coefficient of both quenchers to the lipid bilayers [27]. After each quencher addition, samples were incubated for 10 min before measurement. Quenching data were analyzed by using the Stern–Volmer equation (Eq. (3)), or the Lehrer equation (Eq. (5)) when a negative deviation from the Stern–Volmer relationship is observed. [27,28]

$$\frac{I_0}{I} = \frac{1 + K_{SV} [Q]}{(1 + K_{SV} [Q])(1 - f_b) + f_b} \quad (5)$$

where f_b corresponds to the fraction of light arising from the accessible fluorophores to the quencher.

2.9. Tryptophan fluorescence: red edge effect

Excitation wavelengths from 270 to 310 nm were used to observe an eventual red edge excitation shift effect (REES) [29,30], at 25 °C in the presence of 3 mM LUVs. The emission spectra of LUVs in the same experimental conditions, without peptide, were used for blank subtraction. For the sake of comparison, identical measurements were conducted for 10 μM peptide in buffer.

3. Results

3.1. Surface pressure

The interaction of both peptides with lipid surfaces was first studied by its effect on the monolayers surface pressure change ($\Delta\Pi$) produced by peptides injected in the subphase underneath lipid monolayers stabilized on the air–water interface. As revealed in Fig. 2, $\Delta\Pi$ values resulting from the peptide interaction with PC or PC:PG monolayers at the air–water interface vary with the peptide concentration in the surface. In Fig. 2 (panel A), the effect of 107–115 hLz and [$K^{108}W^{111}$]107–115 hLz on PC monolayers is shown. It can be observed that for a similar degree of coverage (Fig. 2 panel B) the effect on surface pressure is comparable for both peptides. In contrast, the highest changes on surface pressure on charged (PG containing) monolayers were found with [$K^{108}W^{111}$]107–115 hLz (Fig. 2 panel C) for a degree of coverage of 1 (Fig. 2D).

The comparison of data in Fig. 2 denotes that changes produced by both peptides on PC monolayers are similar and quite comparable to that produced by the unmodified peptide on PG containing monolayers. Thus, although the interaction of both peptides with neutral lipids (DMPC) is also feasible, it is strongly enhanced for the novel peptide [$K^{108}W^{111}$]107–115 hLz in the presence of charged lipids. This result highlights that other forces in addition to electrostatic charges drive the peptide insertion and that the peptide substitution at position 111 (Ala by Trp) might affect such non electrostatic contributions.

In order to get an insight on peptide insertion mechanism, we analyze the surface pressure data using the Langmuir isotherm described in Section 2 (Eq. (1)). The comparison of the curves on neutral lipids did not show important differences between the peptides, both giving an n coefficient close to 1, indicating an adsorption in independent sites (Fig. 2B). In contrast, the fitting of the curves corresponding to the adsorption of [$K^{108}W^{111}$]107–115 hLz on charged lipid (PC:PG monolayers) showed a strong deviation from a classical Langmuir adsorption, as denoted by the n coefficient lower than 1, while 107–115 hLz remains with an n value close to 1 (Fig. 2D). The values of n for both peptides in PC and PC:PG monolayers are presented on Table 1.

Significant differences between both peptides were found when the perturbation $\Delta\Pi$ was analyzed at different initial surface pressure using DMPC monolayers (Fig. 3). The limiting surface pressure or exclusion pressure (cut-off) [31,32] was determined by extrapolating the regression of the surface pressure ($\Delta\Pi$) vs. Π_0 plots to the xx axis (Fig. 3). This limiting surface pressure, was defined as the maximum initial surface pressure above which the perturbation of the monolayer does not occurs any more, is a measure of the molecule membrane-penetrating power [33]. In both cases, $\Delta\Pi$ decreases linearly with increasing Π_0, with different slopes, being the exclusion surface pressures 40.39 and 33.43 mN/m for [$K^{108}W^{111}$]107–115 hLz and 107–115 hLz, respectively. The higher slope for the 107–115 hLz in comparison to the modified [$K^{108}W^{111}$]107–115 hLz denotes that the later requires a less hydrated membrane phase. In turn, the higher cut-off indicates that [$K^{108}W^{111}$]107–115 hLz stabilizes in a more expanded interphase [34].

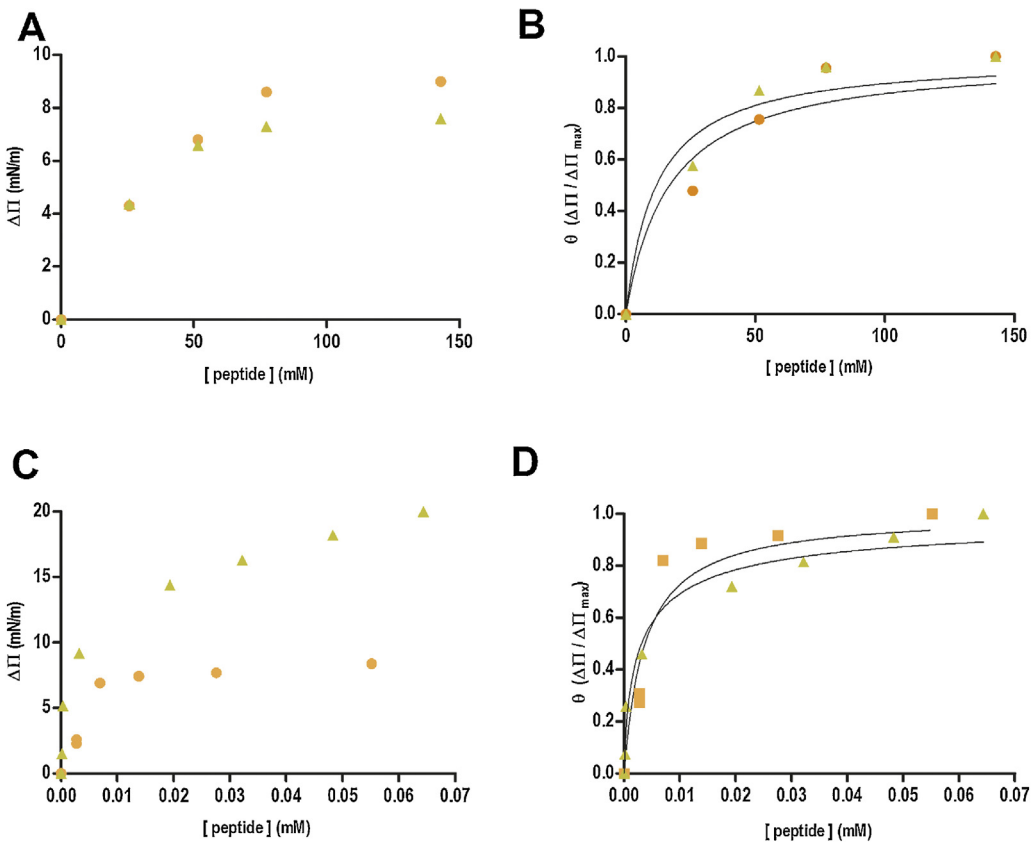

Fig. 2. Interaction of 107–115 hLz (●) and [K^{108}W^{111}]107–115 hLz (▲)with lipid monolayers. Changes in the surface pressure expressed as $\Delta\Pi$ ((A) and (C)) or degree of coverage θ ((B) and (D)) as a function of the peptide concentration on pure DMPC monolayers (A and B) or DMPC:DMPG monolayers ((C) and (D)). The initial pressure was 21 ± 1 mN/m for all assays.

Table 1
Parameters obtained from the fitting of the pressure data of lipid monolayers assays with 107–115 hLz or [K^{108}W^{111}]107–115 hLz using Eqs. (1) and (2). The concentrations of peptide used to determine the *r* coefficient are indicated between brackets. The initial pressure was 21 ± 1 mN/m in all assays.

		107–115 hLz	[K^{108}W^{111}]107–115 hLz
n from Langmuir equation	DMPC	≈1	≈1
	DOPC:DMPG (5:1)	≈1	0.7
Relaxation coefficient (*r*)	DMPC	0.556 (50 mM)	0.699 (50 mM)
	DOPC:DMPG (5:1)	0.581 (0.5 mM)	0.766 (0.5 mM)
	DOPC:DMPG (5:1)	0.592 (0.003 mM)	0.694 (0.028 mM)
	DOPC:DMPG (5:1)	0.484 (0.001 mM)	0.659 (0.017 mM)
	DOPC:DMPG (5:1)	0.566 (4.4 × 10^{-4}mM)	0.381 (3.1 × 10^{-4}mM)

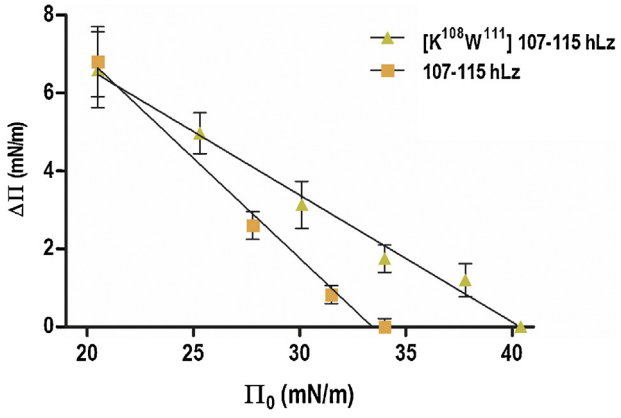

Fig. 3. Changes in surface pressure as a function of the initial surface pressure (Π_0) after the injection of 107–115 hLz or [K^{108}W^{111}]107–115 hLz to reach a final concentration of 50 mM in DMPC monolayers.

3.2. Membrane partition

The different cut off values obtained with 107–115 hLz and [K^{108}W^{111}]107–115 hLz for neutral lipids in Fig. 3 indicate that the peptide interaction depends on the exposure of surface groups to water and hence on the available area on the surface. In addition, the different slope values could indicate that confined water between the acyl chains might be also involved in the interaction [35]. Therefore, the Trp partition in neutral lipid could give us an insight of the non electrostatic interactions. UV–visible absorption and fluorescence spectra in buffer of 107–115 hLz and [K^{108}W^{111}]107–115 hLz are identical to those of Trp in aqueous solution, as expected (Fig. 4A). As shown in Fig. 4B and C, the Trp fluorescence intensity of the peptides increases in the presence of LUV (increased quantum yield). The partition coefficient between the lipid and aqueous phases, K_p, determined by fitting the fluorescence intensity data in eq. 3, are presented in Table 2. For all lipids tested, [K^{108}W^{111}]107–115 hLz exhibited a higher K_p than 107–115 hLz. Both peptides, for negatively charged phospholipids

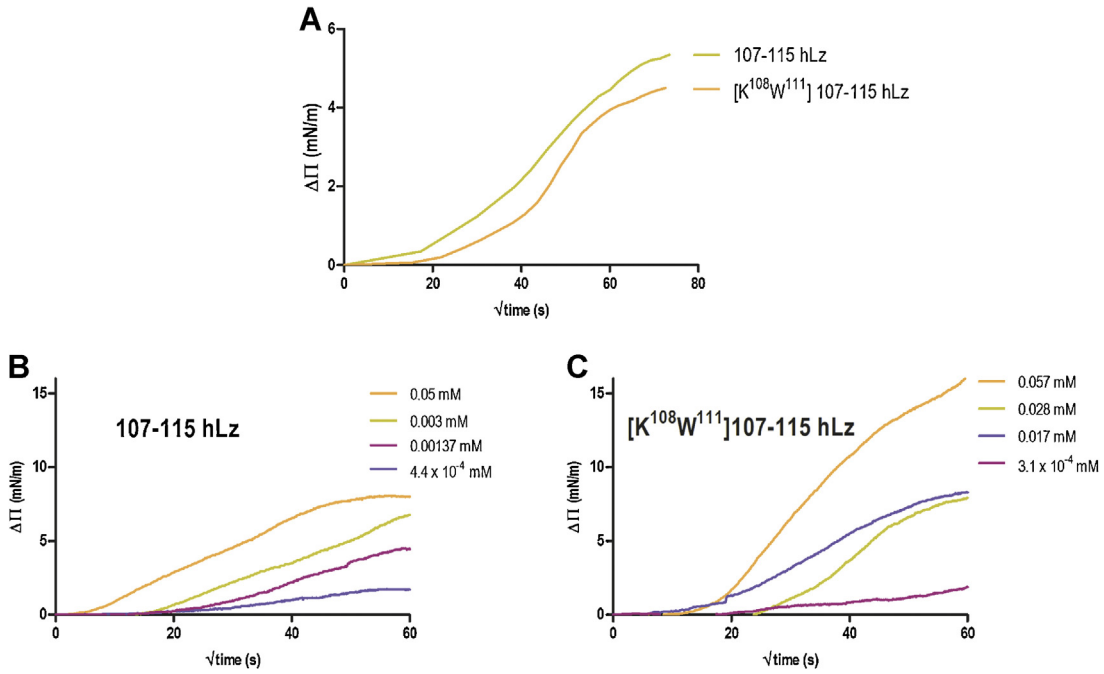

Fig. 4. Variation of the surface pressure as a function of time, after the injection of 107–115 hLz or [$K^{108}W^{111}$]107–115 hLz to reach a final concentration of 50 mM in DMPC (A) or DOPC:DMPG (5:1) ((B) and (C)) monolayers. the initial pressure was 21 ± 1 mN/m for all experiments.

(PG) present higher K_p. However, this effect was more pronounced for [$K^{108}W^{111}$]107–115 hLz. This is a relevant result because PG is the second major phospholipid components of bacterial plasma membranes [36].

These results reveal that PG is relevant to enhance the interaction of both peptides but partition is also feasible in neutral lipids and enhanced in the novel peptide [$K^{108}W^{111}$]107–115 hLz. This means that hydrophobic contacts might play an important role in addition to electrostatic interactions driving to the peptide insertion into the lipidic monolayers. The major difference in the partition process was obtained for [$K^{108}W^{111}$]107–115 hLz in DMPC:DOPG (2.5:1) membranes. This indicates that electrostatic enhances the partition of the modified peptide that are linkable with its improved activity.

3.3. Localization of the peptides in the lipid bilayer

In order to test the accessibility of the fluorophores (Trp in our case) to the aqueous environment, the fluorescence quenching by acrylamide of the Trp residues of both peptides was studied. Acrylamide is an aqueous soluble quencher that presents a low capacity of penetration into lipid bilayers [37]. If a fluorescent molecule inserts in the membrane, it will be less accessible or inaccessible to the quencher in aqueous solution and, therefore, its fluorescence will be less quenched or not quenched at all [38,39].

Linear Stern–Volmer plots were obtained both in the presence and absence of lipids (Fig. 5). Both peptides yielded lower K_{sv} values in the presence of lipids than those obtained in their absence (15.46 ± 0.3 mM^{-1} in solution and 2.72 ± 0.09 mM^{-1} in the presence of LUVs for 107–115 hLz and 17.61 ± 0.4 mM^{-1} in solution and 1.76 ±0.1 mM^{-1} in the presence of LUVs for [$K^{108}W^{111}$]107–115 hLz). Also, the linear plots of fluorescence quenching revealed that no hydrophobic pockets were present. Although the existence of hydrophobic pockets does not seem likely in a small peptide, aggregation or clustering could eventually take place. Aggregation is probably prevented by the positively charged residues of both peptides.

5 and 16NS stearic acid molecules were used to evaluate the in-depth location of the Trp residues of the peptides inserted in PC:PG vesicles. 5NS results a better quencher for molecules inserted in the membrane in a shallow position, close to the lipid–water interface, while 16NS quenches better molecules buried deeply in the membrane [40]. Stern–Volmer plots shown in Fig. 5C and D did not reveal significant differences between both peptides. Fluorescence quenching data enabled the application of the SIMEXDA method [40] to obtain the in-depth distribution of the Trp residues (Fig. 5E). The calculated distance from the center of the bilayer indicates that both peptides are located close to the membrane–water interface. The results denote that once the peptides reach the membrane, Trp belonging to both peptides locates in a similar environment of the membrane. Fig. 5E represents the mean position of 2 Trp in the case of 107–115 hLz and 3 Trp in the case of [$K^{108}W^{111}$] 107–115 hLz. The fact that an additional Trp residue of [$K^{108}W^{111}$]107–115 hLz did not result in a change in the average location could indicate that the 3 Trp residues accommodate at the membrane surface slightly buried a few nm into the bilayer. Single-Trp analogues would allow to accurately determine the insertion depth of each of the Trp residues. However, single-Trp analogues of indolicidin have been demonstrated to have altered biological activity; such studies may not be applicable to the native peptides [41].

Table 2
Partition coefficients obtained from the fitting of the fluorescence assay data of peptides [$K^{108}W^{111}$]107–115 hLz or 107–115 in Eq. (3). All measures were made at least in triplicate. Values are presented as mean ± standard deviation.

	107–115 hLz × 10^3	[$K^{108}W^{111}$]107–115 hLz × 10^3
DMPC	0.2 ± 0.1	3.2 ± 0.8
DMPC:POPG 5:1	1.9 ± 0.1	7.5 ± 1.0
DMPC:POPG 5:2	3.6 ± 0.2	17.3 ± 1.0
POPC:POPG 5:2	6.2 ± 0.4	15.6 ± 1.2

3.4. Kinetic assays

Variations of the surface pressure as a function of time after the injection of 107–115 hLz and [$K^{108}W^{111}$]107–115 hLz in PC

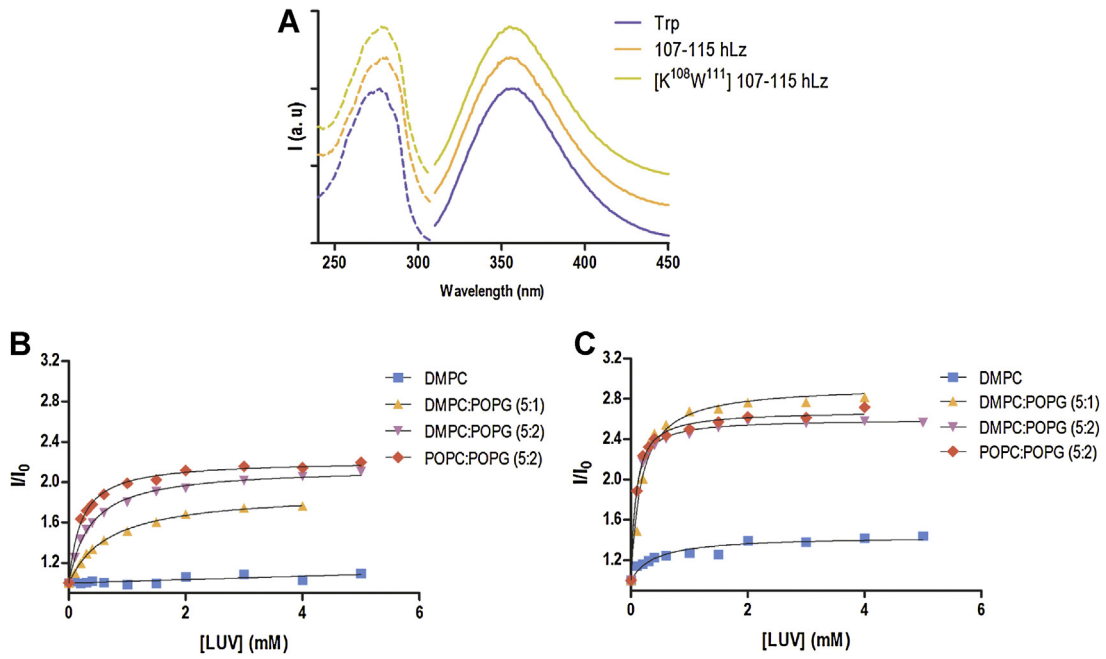

Fig. 5. Normalized fluorescence excitation (dashed line) and emission (solid line) spectra for Trp and peptides 107–115 hLz and [$K^{108}W^{111}$]107–115 hLz in aqueous solution (5 μM) (A). Partition study of the peptides into lipid vesicles. Variation of the fluorescence intensity upon titration with LUV suspensions (composed by different lipids) for peptides 107–115 hLz (B) or [$K^{108}W^{111}$]107–115 hLz (5 μM) (C).

and PC:PG monolayers are shown in Fig. 6. The kinetic pattern of [$K^{108}W^{111}$]107–115 hLz in PC monolayers (panel A) show a deviation of linearity for [$K^{108}W^{111}$]107-115 hLz, absent on the non modified peptide.

On DOPC:DMPG monolayers, the linearity observed at different concentration of 107-115 hLz (panel B) is lost when increasing concentrations of [$K^{108}W^{111}$]107-115 hLz are added to PC:PG monolayers (Panel C).

For a better comparison between the different deviations in the kinetic analysis a relaxation coefficient (r) defined according to Eq. (3) was obtained to characterize the peptide adsorption kinetics. When the r value is close to 0.5 the interactions could be described as *fickeans*, in contrast when the r coefficient departs from 0.5 the interaction could be described as anomalous or *non-Fickean* [42]. In the case of 107–115 hLz for all the conditions assayed the r coefficient remained close to 0.5 (Table 2). On the other hand for [$K^{108}W^{111}$]107–115 hLz the r coefficient values kept away from 0.5 showing a higher distance in PG containing membranes at saturating peptide concentration (Table 1).

3.5. Structural correspondence with relaxation processes. Changes in tryptophan fluorescence excitation: Red edge effect

As already shown, from the adsorption isotherms result n coefficients different from 1; denoting a non-Langmuir behavior for [$K^{108}W^{111}$]107-115 hLz (Fig. 2 and Table 1). This denotes that peptide insertion might be produced with structural rearrangements in the membrane. In addition, as shown in Fig. 6, kinetics of peptide 107–115 hLz follows a *fickean* pattern, while [$K^{108}W^{111}$]107–115 hLz fits within a *non fickean* process (Fig. 6 and Table 1).

Based on the analysis of the adsorption isotherm and the kinetics assays, the insertion of pepetide [$K^{108}W^{111}$]107–115 hLz takes place with changes in membrane structure. In order to explore these changes, the Trp environments of both peptides where analyzed by fluorescence spectroscopy. The influence of the emission wavelength on the excitation wavelength depends on solvent reorientation during the lifetime of the excited fluorophore singlet state [30,43]. For Trp residues imbedded in the less mobile region of the membrane, the red edge effect, i.e., the shift of the emission to higher wavelengths at the red edge of the excitation is stronger. For both peptides in water, there was no significant red edge shift. However, when the peptides were incubated with LUV of DMPC or DMPC:POPG (2.5:1), a red edge shift was observed for both peptides (Fig. 7). [$K^{108}W^{111}$]107-115 hLz reveals a stronger red edge shift with both lipid compositions tested (≈18 and 15 nm for DMPC:POPG and DMPC, respectively) in comparison with 107–115 HLZ (≈11 and 9 nm for DMPC:POPG and DMPC, respectively). As from the result of Trp quenching we are not able to ascribe a particular effect at each Trp, instead we are only able to see the average results that involve all Trp en each peptide. Although the presence of multiple Trp residues makes interpretation of the red edge excitation shift data more uncertain, particularly so in the presence of lipid, we emphasize the trends observed and the comparative behavior among the peptides studied.

4. Discussion

In previous works, it was shown that the understanding of the interaction between AMPs and membranes (using lipid membrane models and blood cells) represent a key aspect to elucidate their mechanism of action [10,44,45]. The membranotropic behavior of a peptide can increase its local concentration at the membrane level, boosting the efficiency of the drug [46]. In this context, we compared the membrane interactions of 107–115 hLz and its analog [$K^{108}W^{111}$]107–115 hLz, in order to understand the molecular basis of its significantly increased antimicrobial efficiency of the later.

This study demonstrates that the substitution of Ala by Lys at position 108 and Ala by Trp at position 111 on the lead peptide results in an increase of membrane affinity, as observed on partition, surface pressure and quenching data (Figs. 2–6). As shown in Table 2, [$K^{108}W^{111}$]107–115 hLz exhibits a higher K_p for all the lipid formulations tested. The increased of the negative membrane charge raises the K_p values of both peptides, as expected, due to the peptides positive net charge, but this effect was stronger for the

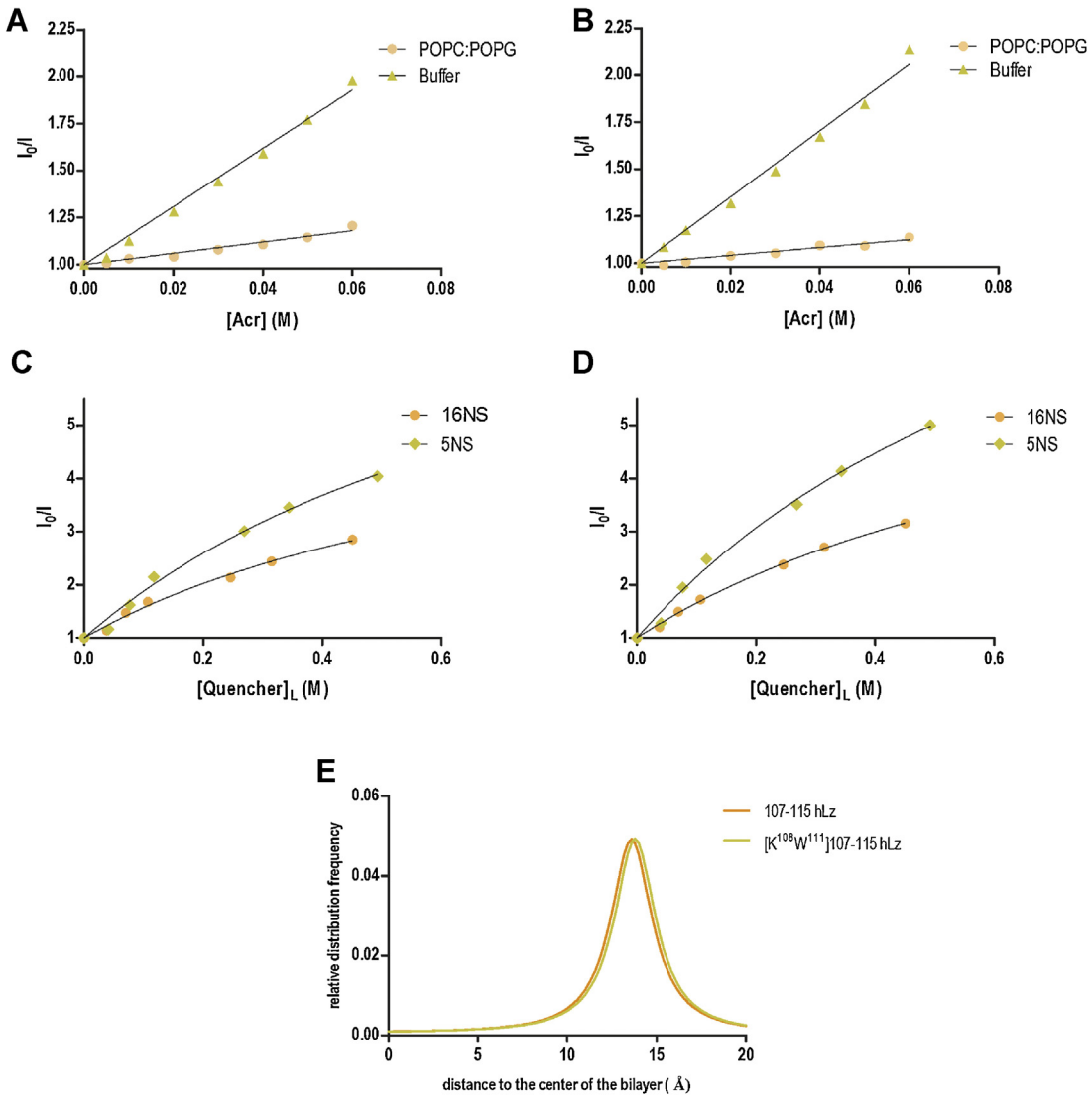

Fig. 6. Localization of the peptides in the bilayer. Fluorescence quenching of 5 μM 107–115 hLz (A) and [K^{108}W^{111}]107–115 hLz (B) by acrylamide in the presence and absence of lipid vesicles. Fluorescence quenching of peptides 107–115 hLz (C) and [K^{108}W^{111}]107–115 hLz (D) peptides by 5NS and 16NS in the bilayer. In-depth localization (E) of both peptides Trp residues of both peptides inside the membrane using the SIMEXDA method [40] yielding an average location 13.6 Å away from the centre of the bilayer for 107–115 hLz and 13.8 for [K^{108}W^{111}]107–115 hLz. Distributions' half-width at half-height were 1.41 Å for both peptides.

peptide [K^{108}W^{111}]107–115 hLz. However, the fact that upon interacting with a zwitterionic membrane (DMPC) [K^{108}W^{111}]107–115 hLz also exhibits a significantly higher K_p means that additionally to the increased positive charges other contributions may enhance the peptide–membrane interactions.

Quantifying the molar fraction (X_L) of the peptide on the membrane [38]

$$X_L = \frac{k_p \gamma_L [L]}{1 + k_p \gamma_L [L]} \quad (6)$$

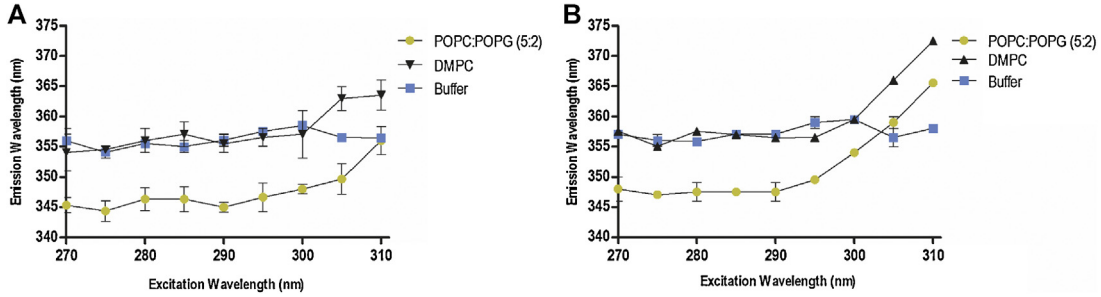

Fig. 7. Red edge excitation shift, for peptides 107–115 hLz (A) and [K^{108}W^{111}]107–115 hLz (B) in buffer and DMPC, POPC:POPG LUVs. (For interpretation of the references to color in this figure legend, the reader is referred to the web version of this article).

we obtained for pure DMPC membrane, working in a lipid high molar excess condition (3 mM), a X_L for 107–115 hLz of 0.32. However, in the same conditions, X_L value for [$K^{108}W^{111}$]107–115 hLz was rised to 0.88, meaning that [$K^{108}W^{111}$]107–115 hLz tends to accumulate in the lipidic environment 2.5-fold higher than the lead peptide. When we move to negatively charged membranes that difference becomes lower but still significant (X_L values of 0.88 for 107–115 hLz and 0.97 for [$K^{108}W^{111}$]107–115 hLz). These further evidences that beside the increased positive charge other factors might promote the peptide membranotropism.

Beside the difference on the membrane affinity of both peptides a different penetration process becomes evident upon comparing the lead peptide with its improved analog, despite the fact that no changes in the final position were detectable (Fig. 5E). On membranes with charged lipid (PG), a deviation from Langmuir adsorption was showed for [$K^{108}W^{111}$]107–115 hLz (Table 1), concomitant with departure of the relaxation coefficient (r) from 0.5 in the kinetic behavior, both differences denote a more complex mechanism instead of a than the single adsorption process observed for 107–115 hLz. A physical interpretation of the relaxation coefficient (r) value can be discussed in terms of normal and anomalous diffusion of the peptides through the membrane. The linearity of the amount of substance adsorbed by a material with the square root of time assumes that the system responds to a linear gradient of concentration across the material in a steady state [47,48]. When the diffusion behavior cannot be described adequately by Fick's law, anomalous or *non-Fickean* diffusion occurs. Deviations from *Fickian* behaviour are considered to be associated with the finite rates at which the surface structure may change in response to the sorption or desorption of penetrant molecules [17]. This phenomena can be interpreted as an activated process in which rearrangement of the cross-linking network in the lipid surface (probably H bonds) is disrupted and re-formed by the peptide insertion [42]. In our context the anomalous diffusion suggests a synergistic effect due to both electrostatic as non-electrostatic forces that could induce a combined reorganization of the membrane along the membrane–peptide interaction.

Finally, we observed a stronger REES for [$K^{108}W^{111}$]107–115 hLz when compared with 107–115 hLz. This may be due to a more stable insertion of the Trp at the interface level that restrict its mobility [49]. The additional Trp residue might be involved in a higher stabilization of the peptide in the membrane. These results indicate that at the end of the insertion process, the Trp microenvironment of peptide [$K^{108}W^{111}$]107–115 hLz outcomes different from that found by the lead peptide. However, the PC:PG membranes quenching results show that both peptides were located at the same interfacial position, with a average location of all Trp slightly buried 5–6 nm in the membrane, in good agreement with the Trp location of indolicidin, an extended CAMP isolated from the cytoplasmic granules of bovine neutrophiles, which presents high sequence homology and similar far-UV CD spectra with [$K^{108}W^{111}$]107–115 hLz [14,50,51]. Taking this into account, the difference on the REES could be explained by the modification on the membrane induced by peptide [$K^{108}W^{111}$]107–115 hLz, which were not observable for 107–115 hLz, as the pressure data denotes.

In general, CAMPs interact with membranes by a variety of mechanisms which might cause the disruption of the bilayer structure or the loss of the membrane permeability. Several reports have indicated that several CAMPs starting interactions (i.e., at low concentrations of membrane-bound peptide) occur primarily near the membrane surface, with the peptide aligned parallel to the plane of the bilayer in a carpet like manner [52–57]. Peptide insertion near the lipid–water interface was postulated to result in the expansion of the outer leaflet of the bilayer, with continue accumulation of bound peptide, leading to membrane thinning as a prelude to pore formation or detergent-like disintegration of the bilayer [58–61]. According to our results, we propose that peptide [$K^{108}W^{111}$]107–115 hLz binds to the membrane through a process governed by electrostatic forces, followed by the insertion of the Trp residues in the carbon-chain region of the membrane, stabilizing the interaction [62] probably by an initial parallel alignment of the peptide in the membrane, in good agreement with previously reports for related AMPs [50] that promote changes in the lipid organization; triggering the antimicrobial activity. That hypothesis are good agreement with recent results from far-UV CD spectra obtained from [$K^{108}W^{111}$]107–115 hLz similar to that obtained for indolicidin [63]. The overall shape of CD spectra reveals that peptide [$K^{108}W^{111}$] 107–115 hLz, and 2 analogs adopted a predominant random coil conformation in water. However, 2 distinctive bands at 200 and 220 nm suggest a decreased content of disordered structure for peptide [$K^{108}W^{111}$] 107–115 hLz [51]. Based on the CD spectra recorded in the presence of TFE and lipidic micelles, we propose that peptide [$K^{108}W^{111}$]107–115 hLz forms a U-shaped amphipathic structure showing a distinct segregation of a hydrophobic core (WVWW) flanked by positively charged hydrophilic regions at both peptide termini (RK and RNR). This conformation may improve the interaction with the microbial plasma membrane and its partitioning at the interface.

In conclusion, the increased activity of [$K^{108}W^{111}$]107–115 hLz peptide might be explained by a synergistic effect between the increased electrostatic forces (substitution of Ala by Lys at position 108), as well as increased hydrophobic interactions (substitution of Ala by Trp at position 111). A recent study on indolocidin confirms that electrostatic indolicidin–membrane interactions are not the sole contributors to the free energy of adsorption. Instead, a balance between an attractive van der Waals enthalpic component and a repulsive entropic component determine the overall strength of the indolicidin adsorption [50].

Acknowledgments

This work was supported with funds from Agencia Nacional de Promoción Cientiífica y Tecnológica, PICT 2007-757, PICT 2011-2606, CONICET (PIP 2011-2013 GI 11220100100484), UBACyT (20020090200663), (Programa-UNSE 23/A164), Fundação para a Ciência e a Tecnologia—Ministério da Educação e Ciência (FCT-MEC, Portugal), and FP7-PEOPLE IRSES (International Research Staff Exchange Scheme, European Union) project MEMPEPACROSS. EAD, NI, OC and AH are members of the Research Career of CONICET (Consejo Nacional de Investigaciones Científicas y Técnicas de la República Argentina). AB is recipient of a post doctoral fellowship of CONICET. AH is recipient of a post doctoral fellowship of FCT-MEC (SFRH/BPD/72037/2010). The authors thank Chemo-Romikin SA (Argentina) for use of their Peptide Synthesizer facilities.

References

[1] A. Menendez, R.B. Ferreira, B.B. Finlay, Defensins keep the peace too, Nat. Immunol. 11 (2010) 49–50.
[2] R.E. Hancock, G. Diamond, The role of cationic antimicrobial peptides in innate host defences, Trends Microbiol. 8 (2000) 402–410.
[3] T. Ganz, Defensins: antimicrobial peptides of innate immunity, Nat. Rev. Immunol. 3 (2003) 710–720.
[4] B. Rivas-Santiago, C.J. Serrano, J.A. Enciso-Moreno, Susceptibility to infectious diseases based on antimicrobial peptide production, Infect. Immun. 77 (2009) 4690–4695.
[5] N. Papo, Y. Shai, Can we predict biological activity of antimicrobial peptides from their interactions with model phospholipid membranes? Peptides 24 (2003) 1693–1703.
[6] A. Giuliani, G. Pirri, S. Nicoletto, Antimicrobial peptides: an overview of a promising class of therapeutics, Cent. Eur. J. Biol. 2 (2007) 1–33.
[7] Y.J. Gordon, E.G. Romanowski, A.M. McDermott, A review of antimicrobial peptides and their therapeutic potential as anti-infective drugs, Curr. Eye Res. 30 (2005) 505–515.
[8] A.M. McDermott, Cationic antimicrobial peptides. A future therapeutic option? Arch. Soc. Esp Oftalmol. 82 (2007) 467–470.

[9] L. Zhang, T.J. Falla, Cationic antimicrobial peptides—an update, Expert Opin. Invest. Drugs 13 (2004) 97–106.
[10] M.M. Domingues, R.G. Inacio, J.M. Raimundo, M. Martins, M.A. Castanho, N.C. Santos, Biophysical characterization of polymyxin B interaction with LPS aggregates and membrane model systems, Biopolymers 98 (2012) 338–344.
[11] M.N. Melo, M.A. Castanho, The mechanism of action of antimicrobial peptides: lipid vesicles vs. bacteria, Front. Immunol. 3 (2012) 236.
[12] W.C. Wimley, K. Hristova, Antimicrobial peptides: successes, challenges and unanswered questions, J. Membr. Biol. 239 (2011) 27–34.
[13] H.R. Ibrahim, U. Thomas, A. Pellegrini, A helix-loop-helix peptide at the upper lip of the active site cleft of lysozyme confers potent antimicrobial activity with membrane permeabilization action, J. Biol. Chem. 276 (2001) 43767–43774.
[14] R. González, F. Albericio, O. Cascone, N.B. Iannucci, Improved antimicrobial activity of h-lysozyme (107–115) by rational Ala substitution, J. Pept. Sci. 16 (2010) 424–429.
[15] K.J. Williams, R.P. Bax, Challenges in developing new antibacterial drugs, Curr. Opin. Invest. Drugs 10 (2009) 157–163.
[16] S.A. Kates, F. Albericio, Solid-Phase Synthesis A Practical Guide, CRC, Press, Boca Raton, 2000.
[17] J. Crank, The mathematics of diffusion, Oxford University Press, Oxford, 1975.
[18] M. Kubista, R. Sjoback, S. Eriksson, B. Albinsson, Experimental correction for the inner-filter effect in fluorescence spectra, Analyst 119 (1994) 417–419.
[19] A.S. Ladokhin, S. Jayasinghe, S.H. White, How to measure and analyze tryptophan fluorescence in membranes properly, and why bother? Anal. Biochem. 285 (2000) 235–245.
[20] L.D. Mayer, M.J. Hope, P.R. Cullis, Vesicles of variable sizes produced by a rapid extrusion procedure, BBA 858 (1986) 161–168.
[21] F. Szoka, F. Olson, T. Heath, W. Vail, E. Mayhew, D. Papahadjopoulos, Preparation of unilamellar liposomes of intermediate size (0.1–0.2 μmol) by a combination of reverse phase evaporation and extrusion through polycarbonate membranes, BBA 601 (1980) 559–571.
[22] N.C. Santos, M. Prieto, M.A. Castanho, Quantifying molecular partition into model systems of biomembranes: an emphasis on optical spectroscopic methods, BBA 1612 (2003) 123–135.
[23] S.W. Chiu, S. Subramaniam, E. Jakobsson, Simulation study of a gramicidin/lipid bilayer system in excess water and lipid. II. Rates and mechanisms of water transport, Biophys. J. 76 (1999) 1939–1950.
[24] H.G. Franquelim, L.M. Loura, N.C. Santos, M.A. Castanho, Sifuvirtide screens rigid membrane surfaces. establishment of a correlation between efficacy and membrane domain selectivity among HIV fusion inhibitor peptides, J. Am. Chem. Soc. 130 (2008) 6215–6223.
[25] N.C. Santos, M. Castanho, Fluorescence spectroscopy methodologies on the study of proteins and peptides. On the 150th anniversary of protein fluorescence, Trends Appl. Spectrosc. 4 (2002) 113–125.
[26] M. Yamazaki, M. Miyazu, T. Asano, A. Yuba, N. Kume, Direct evidence of induction of interdigitated gel structure in large unilamellar vesicles of dipalmitoylphosphatidylcholine by ethanol: studies by excimer method and high-resolution electron cryomicroscopy, Biophys. J. 66 (1994) 729–733.
[27] N.C. Santos, M. Prieto, M.A.R.B. Castanho, Interaction of the major epitope region of HIV protein gp41 with membrane model systems. A fluorescence spectroscopy study, Biochemistry 37 (1998) 8674–8682.
[28] J.F. Nagle, M.C. Wiener, Structure of fully hydrated bilayer dispersions, BBA 942 (1988) 1–10.
[29] A. Chattopadhyay, Exploring membrane organization and dynamics by the wavelength-selective fluorescence approach, Chem. Phys. Lipids 122 (2003) 3–17.
[30] S. Mukherjee, A. Chattopadhyay, Wavelength-selective fluorescence as a novel tool to study organization and dynamics in complex biological systems, J. Fluoresc. 5 (1995) 237–246.
[31] M. Eeman, A. Berquand, Y.F. Dufrêne, M. Paquot, S. Dufour, M. Deleu, Penetration of surfactin into phospholipid monolayers: nanoscale interfacial organization, Langmuir 22 (2006) 11337–11345.
[32] K.L. Gillotte, M. Zaiou, S. Lund-Katz, G.M. Anantharamaiah, P. Holvoet, A. Dhoest, M.N. Palgunachari, J.P. Segrest, K.H. Weisgraber, G.H. Rothblat, M.C. Phillips, Apolipoprotein-mediated plasma membrane microsolubilization, J. Biol. Chem. 274 (1999) 2021–2028.
[33] W. van Klompenburg, M. Paetzel, J.M. de Jong, R.E. Dalbey, R.A. Demel, G. von Heijne, B. de Kruijff, Phosphatidylethanolamine mediates insertion of the catalytic domain of leader peptidase in membranes, FEBS Lett. 431 (1998) 75–79.
[34] E.A. Disalvo, A. Hollmann, L. Semorile, M.F. Martini, Evaluation of the Defay–Prigogine model for the membrane interphase in relation to biological response in membrane–protein interactions, BBA 1828 (2013) 1834–1839.
[35] E.A. Disalvo, A.M. Bouchet, M.A. Frias, Connected and isolated CH populations in acyl chains and its relation to pockets of confined water in lipid membranes as observed by FTIR spectrometry, BBA 1828 (2013) 1683–1689.
[36] M.M. Domingues, S.C. Lopes, N.C. Santos, A. Quintas, M.A. Castanho, Fold-unfold transitions in the selectivity and mechanism of action of the N-terminal fragment of the bactericidal/permeability-increasing protein (rBPI(21)), Biophys. J. 96 (2009) 987–996.
[37] F. Moro, F.M. Goni, M.A. Urbaneja, Fluorescence quenching at interfaces and the permeation of acrylamide and iodide across phospholipid bilayers, FEBS Lett. 330 (1993) 129–132.
[38] M. Castanho, M. Prieto, Filipin fluorescence quenching by spin-labeled probes: studies in aqueous solution and in a membrane model system, Biophys. J. 69 (1995) 155–168.
[39] M.A. Castanho, M.J. Prieto, Fluorescence quenching data interpretation in biological systems. The use of microscopic models for data analysis and interpretation of complex systems, BBA 1373 (1998) 1–16.
[40] M.X. Fernandes, J. Garcia de la Torre, M.A.R.B. Castanho, Joint determination by Brownian dynamics and fluorescence quenching of the in-depth location profile of biomolecules in membranes, Anal. Biochem. 307 (2002) 1–12.
[41] C. Subbalakshmi, E. Bikshapathy, N. Sitaram, R. Nagaraj, Antibacterial and hemolytic activities of single tryptophan analogs of indolicidin, Biochem. Biophys. Res. Commun. 274 (2000) 714–716.
[42] A. Hollmann, L. Delfederico, G. De Antoni, L. Semorile, E.A. Disalvo, Relaxation processes in the adsorption of surface layer proteins to lipid membranes, J. Phys. Chem. B 114 (2010) 16618–16624.
[43] A.K. Ghosh, R. Rukmini, A. Chattopadhyay, Modulation of tryptophan environment in membrane-bound melittin by negatively charged phospholipids: implications in membrane organization and function, Biochemistry 36 (1997) 14291–14305.
[44] M.M. Domingues, M.A. Castanho, N.C. Santos, rBPI(21) promotes lipopolysaccharide aggregation and exerts its antimicrobial effects by (hemi)fusion of PG-containing membranes, PLoS One 4 (2009) e8385.
[45] S.T. Henriques, M.N. Melo, M.A. Castanho, How to address CPP and AMP translocation? Methods to detect and quantify peptide internalization in vitro and in vivo (review), Mol. Membr. Biol. 24 (2007) 173–184.
[46] M.A. Castanho, M.X. Fernandes, Lipid membrane-induced optimization for ligand-receptor docking: recent tools and insights for the membrane catalysis model, Eur. Biophys. J. 35 (2006) 92–103.
[47] M.F. Martini, E.A. Disalvo, Superficially active water in lipid membranes and its influence on the interaction of an aqueous soluble protease, BBA 1768 (2007) 2541–2548.
[48] H. Sanabria, Y. Kubota, M.N. Waxham, Multiple diffusion mechanisms due to nanostructuring in crowded environments, Biophys. J. 92 (2007) 313–322.
[49] D.J. Schibli, R.F. Epand, H.J. Vogel, R.M. Epand, Tryptophan-rich antimicrobial peptides: comparative properties and membrane interactions, Biochem. Cell Biol. 80 (2002) 667–677.
[50] I.C. Yeh, D.R. Ripoll, A. Wallqvist, Free energy difference in indolicidin attraction to eukaryotic and prokaryotic model cell membranes, J. Phys. Chem. B 116 (2012) 3387–3396.
[51] N.B. Iannucci, L.M. Curto, F. Albericio, O. Cascone, J.M. Delfino, Structural glance into a novel anti-staphylococcal peptide, Biopolymers (2013).
[52] L. Silvestro, P.H. Axelsen, Membrane-induced folding of cecropin A, Biophys. J. 79 (2000) 1465–1477.
[53] K.A. Henzler Wildman, D.K. Lee, A. Ramamoorthy, Mechanism of lipid bilayer disruption by the human antimicrobial peptide, LL-37, Biochemistry 42 (2003) 6545–6558.
[54] K. Bhargava, J.B. Feix, Membrane binding, structure, and localization of cecropin-mellitin hybrid peptides: a site-directed spin-labeling study, Biophys. J. 86 (2004) 329–336.
[55] B. Bechinger, The structure, dynamics and orientation of antimicrobial peptides in membranes by multidimensional solid-state NMR spectroscopy, BBA 1462 (1999) 157–183.
[56] A. Ramamoorthy, S. Thennarasu, D.K. Lee, A. Tan, L. Maloy, Solid-state NMR investigation of the membrane-disrupting mechanism of antimicrobial peptides MSI-78 and MSI-594 derived from magainin 2 and melittin, Biophys. J. 91 (2006) 206–216.
[57] H. Sato, J.B. Feix, Peptide–membrane interactions and mechanisms of membrane destruction by amphipathic alpha-helical antimicrobial peptides, BBA 1758 (2006) 1245–1256.
[58] M.T. Lee, F.Y. Chen, H.W. Huang, Energetics of pore formation induced by membrane active peptides, Biochemistry 43 (2004) 3590–3599.
[59] W.T. Heller, A.J. Waring, R.I. Lehrer, T.A. Harroun, T.M. Weiss, L. Yang, H.W. Huang, Membrane thinning effect of the beta-sheet antimicrobial protegrin, Biochemistry 39 (2000) 139–145.
[60] F.-Y. Chen, M.-T. Lee, H.W. Huang, Evidence for membrane thinning effect as the mechanism for peptide-induced pore formation, Biophys. J. 84 (2003) 3751–3758.
[61] A. Mecke, D.-K. Lee, A. Ramamoorthy, B.G. Orr, M.M. Banaszak Holl, Membrane thinning due to antimicrobial peptide binding: an atomic force microscopy study of MSI-78 in lipid bilayers, Biophys. J. 89 (2005) 4043–4050.
[62] F.E. Herrera, A. Bouchet, F. Lairion, E.A. Disalvo, S. Pantano, Molecular dynamics study of the interaction of arginine with phosphatidylcholine and phosphatidylethanolamine bilayers, J. Phys. Chem. B 116 (2012) 4476–4483.
[63] A. Rozek, C.L. Friedrich, R.E. Hancock, Structure of the bovine antimicrobial peptide indolicidin bound to dodecylphosphocholine and sodium dodecyl sulfate micelles, Biochemistry 39 (2000) 15765–15774.
[64] M.E. Selsted, M.J. Novotny, W.L. Morris, Y.Q. Tang, W. Smith, J.S. Cullor, Indolicidin, a novel bactericidal tridecapeptide amide from neutrophils, J. Biol. Chem. 267 (1992) 4292–4295.